Letter Vol. 4, No. 12 / December 2017 / Optica 1522

optica

Ultrahigh-transparency, ultrahigh-haze nanograss glass with fluid-induced switchable haze

Sajad Haghanifar,[1] Tongchuan Gao,[1] Rafael T. Rodriguez De Vecchis,[2] Bradley Pafchek,[2] Tevis D. B. Jacobs,[2] and Paul W. Leu[1,2,*]

[1]Department of Industrial Engineering, University of Pittsburgh, Pittsburgh, Pennsylvania 15261, USA
[2]Department of Mechanical Engineering and Materials Science, University of Pittsburgh, Pittsburgh, Pennsylvania 15261, USA
*Corresponding author: pleu@pitt.edu

Received 29 August 2017; revised 11 November 2017; accepted 12 November 2017 (Doc. ID 305778); published 12 December 2017

Optoelectronic applications such as solar cells and light-emitting diodes would benefit from glass substrates with both high transparency and high haze to improve power conversion and extraction efficiencies, respectively. In this Letter, we demonstrate glass with grass-like nanostructures that displays ultrahigh transparency and ultrahigh haze (both over 95% at wavelength 550 nm). The nanograss is fabricated by a scalable maskless reactive ion etching process in fused silica where the height is controlled via the etch time. We demonstrate that shorter nanograss (<2.5 μm height) improves the antireflection properties of the glass and that longer grass tends to increase haze monotonically. Ultrahigh haze, over 99%, may also be achieved with longer nanograss (>6 μm height), though the transmission decreases slightly to less than 92%. Finally, we demonstrate that various fluids with a similar index of refraction as the glass may be used to switch the haze of these substrates.

OCIS codes: (290.0290) Scattering; (290.5880) Scattering, rough surfaces; (310.1210) Antireflection coatings; (050.6624) Subwavelength structures; (130.4815) Optical switching devices.

https://doi.org/10.1364/OPTICA.4.001522

Glass substrates form a critical component in many optoelectronic devices, such as displays, lighting, solar cells, smartphones, tablets, and e-paper, where the glass must protect the device from the ambient environment and allow light to pass through and couple into or out of the active layers of the device. Typically, glass has a quarter-wave thickness antireflection layer coating in order to reduce reflection losses at the air/glass interface [1]. In addition to these functionalities, many optoelectronic applications such as solar cells [2,3], backlit liquid crystal displays [4], and light-emitting diodes (LEDs) [5,6] would benefit from glass substrates with both high transparency and high haze. Substrates with high haze can increase how much light scatters into or out of the underlying photoactive layers [7] and may increase the solar cell power conversion efficiency or LED extraction efficiency, respectively. For example, Fang *et al.* recently introduced a transparent paper fabricated using wood fibers, that possesses both ultrahigh transmission (96%) and high haze (60%), and showed that this paper can increase solar cell efficiency [8]. Finally, optical switchability is desired in a variety of smart glass window applications, where this functionality may be utilized to affect temperature, comfort, and privacy [9–11]. A variety of active approaches such as electrochromism [12–14] and liquid crystal alignment [15,16] have been demonstrated for optical switchability, though these approaches still face many technological and economic barriers to widespread adoption.

In this Letter, we demonstrate monolithic fused silica nanograss glass with both ultrahigh transparency and ultrahigh haze (both over 95% at 550 nm wavelength). The nanograss is fabricated through a scalable maskless one-step reactive ion etching (RIE) process on fused silica glass where the height is controlled through the etch time. We demonstrate that shorter grass (<2.5 μm) improves the antireflection properties of the glass, but the antireflection decreases at larger heights due to increased scattered (or diffuse) reflectance. In contrast, longer grass tends to monotonically increase the haze. Finally, we demonstrate that the nanograss glass is superhydrophilic. Various fluids with a similar index of refraction as the glass may be utilized to permeate the nanograss, such that it resembles a uniform flat glass substrate with little haze. Upon removal of the fluid, the nanograss recovers its original hazy state.

Figure 1 shows scanning electron microscopy (SEM) images of the sub-wavelength nanograss glass. The nanograss is fabricated by a maskless RIE fabrication process (Trion Technology Phantom III) [17]. The fused silica is etched by CHF_3, SF_6, and Ar at 40, 10, and 85 sccm flow rates, respectively. The total pressure of chamber was kept at 200 mTorr, and the power was 300 W. During the etching process, polymer particles are deposited on the surface of the fused silica substrate, which acts as a micro-mask and allows the etching to create the high-aspect-ratio nanograss [18]. Seven glass substrates were etched for 20, 80, 100, 150, 200, 300, and 450 min, yielding nanograss with heights of 0.8, 2.5, 3.3, 4.5, 5.2, 6.0, and 8.5 μm, respectively. Figure 1(a) shows cross-section SEM images of the (i) 2.5, (ii) 4.5, (iii) 6, and (iv) 8.5 μm height nanograss. The etch rate is approximately 16 nm/min for a several square centimeters (cm^2) area,

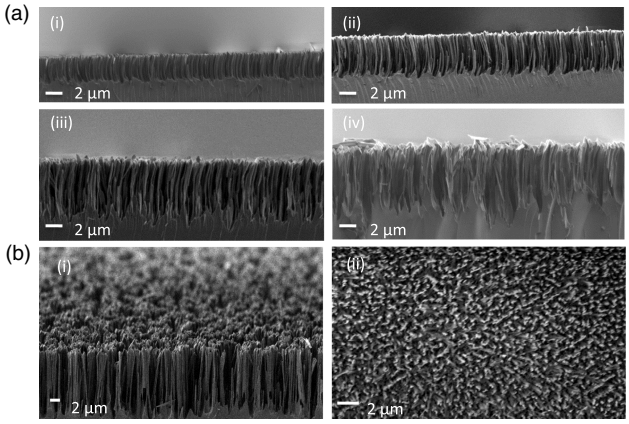

Fig. 1. (a) Cross-section SEM images of nanostructured grass-like glass with (i) 2.5, (ii) 4.5, (iii) 6, and (iv) 8.5 μm height, and (b) (i) 15° tilted and (ii) overhead view of 6 μm height hazy glass.

500 μm thick chip. Figure 1(b) (i) and (ii) show 15° tilted and overhead-view SEM images of the 6 μm nanograss glass, respectively. The diameter of each grass blade is roughly 100–200 nm, and the distance between adjacent grass blades is approximately 100–700 nm. The surface is etched uniformly over the entire glass substrate.

The total and direct (or specular) transmissions of all nanograss samples as well as smooth glass were measured using an ultra-violet (UV), visible (vis) and near infra-red (NIR) spectrophotometer (PerkinElmer, Lambda 750) with and without an integrating sphere, respectively. Figure 2 plots the contour of (a) total transmission and (b) haze factor spectra of different height nanograss glass ranging in height from 0 to 8.5 μm over wavelengths of 250–1200 nm. The haze factor is defined as the percent of scattered transmission to the total transmission,

$$H(\lambda) = \left(1 - \frac{\text{direct transmission}(\lambda)}{\text{total transmission}(\lambda)}\right) \times 100\%, \quad (1)$$

where haze is represented by H and λ is the free-space wavelength. For the entire spectrum, the smooth glass has a haze of less than 2.5% and a total transmission of about 93.5%. For the 2.5 μm height nanograss, the transmission spectra remains fairly flat and is an improvement over that of the smooth glass. However, as the nanograss continues to increase in height, the total transmission tends to decrease, particularly more at shorter wavelengths. In contrast, the haze tends to decrease at longer wavelengths. The scattering of near-infrared photons (wavelength 750–1110 nm) would benefit thin silicon solar cells by scattering light into the silicon [19,20]. The high-haze nanograss may help to overcome silicon's low absorption near its band-gap energy.

Next, we focus our discussion on how the nanograss height affects the transmission and haze of 550 nm wavelength light, which is the average wavelength of visible light. Figure 3 plots the results of the total transmission and haze at this wavelength as a function of nanograss height. Smooth glass has a transmission of 93.5%. Low-height nanograss increases the transmission due to improved antireflection. We find a maximum transmission of 97.0% for 2.5 μm height nanograss before the transmission decreases at larger heights due to increased scattered (or diffuse) reflection. In contrast, the haze increases monotonically with increasing height as the scattering probability of the light increases. While the smooth glass has a haze of only 0.8%, this haze increases to 1.7% for 0.8 μm nanograss, and haze factors over 99% may be achieved with nanograss above 6 μm height.

To explain our haze results, we compare our results with the haze predicted from scalar scattering theory of a single rough surface where the height of the surface has a Gaussian distribution [21,22]. According to this theory, the wavelength-dependent haze at normal angle of incidence is

$$H(\lambda) = \left(1 - \exp\left[-\left(\frac{2\pi\sigma_{\text{rms}}[n_1 - n_2(\lambda)]}{\lambda}\right)^2\right]\right) \times 100\%, \quad (2)$$

where root mean square roughness of the surface and the refractive indices of the two media on either side of the interface are represented by σ_{rms}, n_1, and $n_2(\lambda)$, respectively. In our case, $n_1 = 1$ for air, and n_2 varies from 1.51 at 250 nm to 1.45 at 1200 nm for fused silica [23]. This theory assumes that the surface correlation length is much larger than the root mean square roughness and does not consider multiple scattering.

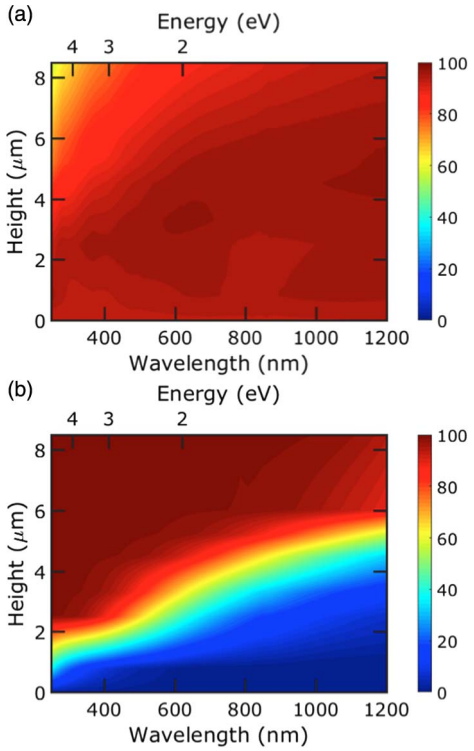

Fig. 2. Contour plots of (a) total transmission (%) and (b) haze (%) as a function of wavelength and nanograss height.

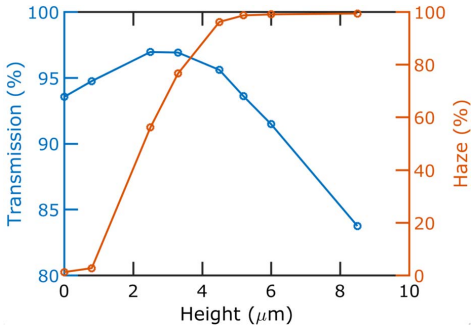

Fig. 3. Plots of total transmission (left y axis) and haze (right y axis) at 550 nm wavelength as a function of nanograss height.

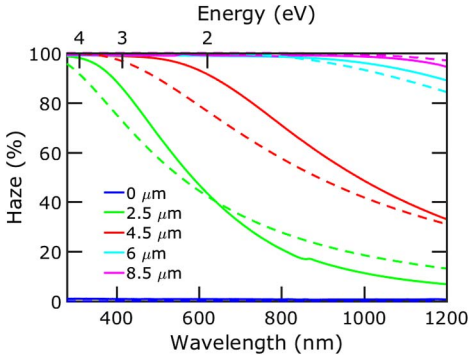

Fig. 4. Experimental (solid lines) and scalar scattering theory (dashed lines) haze values for smooth glass and glass with 2.5, 4.5, 6, and 8.5 μm height nanograss.

This equation has been used to model scattering in thin-film solar cells [21,24–26].

Optical profilometry (Contour GT Bruker) was used to measure the root mean square roughnesses of the hazy glass. σ_{rms} equal to 160, 260, 580, and 800 nm were measured for the hazy glass with heights of 2.5, 4.5, 6, and 8.5 μm, respectively (Fig. S1, Supplement 1). Figure 4 plots our experimental haze results compared to those predicted from Eq. (2). The scalar scattering theory results match well with experimental results, though some differences are seen due to the lack of considering multiple scattering from surfaces in the theory.

Figure 5 shows optical images of smooth fused silica and fused silica with various height nanograss when the substrate is (a) placed directly on top of the text and (b) placed about 1 cm above the text (Fig. S2 in Supplement 1 is the complete version). When the substrate is placed directly on the text, the differences in visible transmission of the various samples are apparent. When the substrate is held about 1 cm above the text, the increasing haze with increasing height can be observed. Even though the 6 μm height nanograss glass looks opaque, in fact, it is only the direct transmission that is low; its total transmission is 91.5% at 550 nm, which is only slightly lower than the 93.5% of smooth glass.

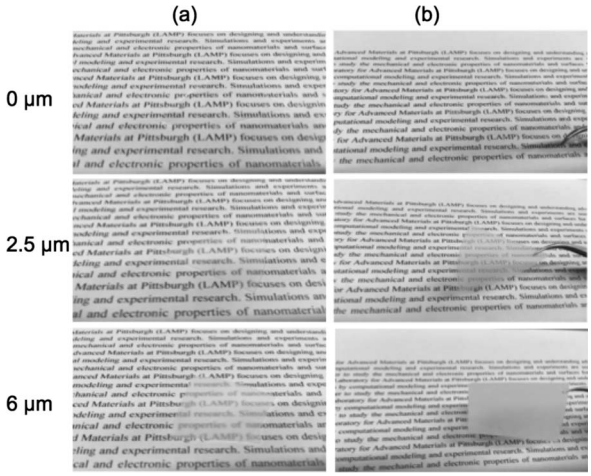

Fig. 5. Optical images of smooth glass and glass with 2.5 and 6 μm height nanograss when placed (a) directly on paper with text and (b) about 1 cm above.

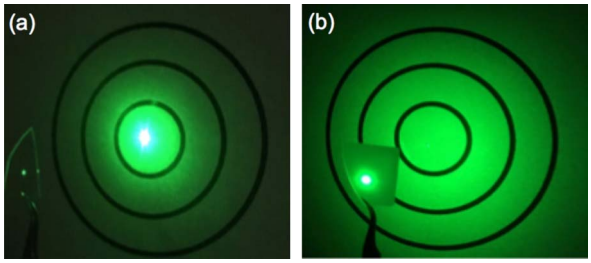

Fig. 6. Scattering ability of (a) flat fused silica and (b) 6 μm height nanograss glass. The scattering ability is demonstrated by shining a laser through a sample onto a target. The rings on the target are spaced 5 cm apart. The distance between the sample and target is 30 cm.

The scattering of light is shown in Fig. 6. A green laser beam with a wavelength 532 nm was used to visualize the light scattering ability of the (a) flat fused silica and (b) 6 μm height nanograss glass. The transmitted light passing through the flat fused silica shows a small luminous radius on the target with high intensity. The light scattering and haze of the flat fused silica is low. In contrast, for the 6 μm height nanograss, the light passing through the sample is almost completely scattered with no observation of a central point on the target. The smooth fused silica is hydrophilic. The static water contact angle (WCA) of flat fused silica is 46 ± 1.5° [Fig. 7(a)(i)]. Due to the hydrophilicity of the surface, water easily fills the empty spaces between the blades of the grass and spreads across the surface. Nanostructures enhance the hydrophilicity or hydrophobicity of a surface when the wetting is in the Wenzel state [27]. For the 6 μm nanograss glass, the static WCA is 7 ± 1.5° [Fig. 7(a)(ii)]. Consequently, since the refractive index of the water (1.33 at 550 nm [23]) is near that of the fused silica (1.46 at 550 nm [23]), the glass has low haze when it is wet by the liquid. Optical images are shown in Fig. 7(b) of the transition between transparent and haze modes of 6 μm nanograss glass that occurs when water is applied. When the surface is wet, the water fills the gaps and the glass has low haze (0 s). As the water is removed (in this case, from evaporation), the haziness increases, and after about 80 s, the glass returns to its original hazy state. Figure S3 in Supplement 1 shows additional images at times in between.

We characterize the transmission properties of the nanograss glass when wet by different liquids—water, acetone, and toluene—in the 350–850 nm wavelength range. The wavelength range is

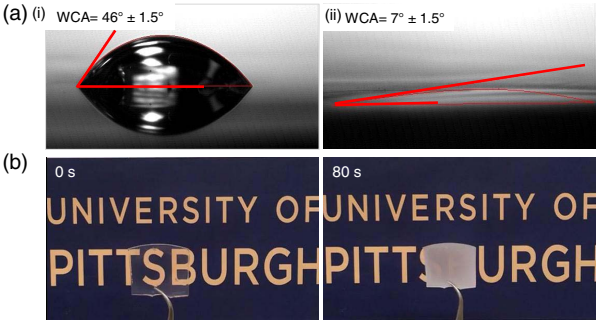

Fig. 7. (a) Contact angle of water droplet on (i) smooth fused silica and (ii) 6 μm nanograss glass. (b) Transition between transparent and haze mode of 6 μm ultrahazy glass by putting water on the glass and evaporation in 80 s.

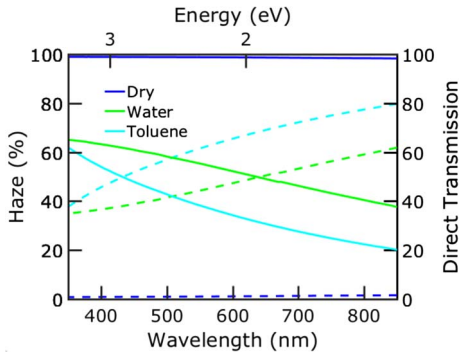

Fig. 8. Haze (solid lines) and direct transmission (dashed lines) as a function of wavelength for 6 μm hazy glass in dry state and wet state with different liquids.

restricted to this range since the cuvette we used (FireflySci Type 523 Rectangular Absorption Cuvette) for characterization is designed for this wavelength range. The refractive indices of these fluids are 1.33, 1.36, and 1.50, respectively, compared to 1.46 for the fused silica at 550 nm wavelength [23]. Figure 8 plots the haze (left y axis) and direct transmission (right y axis) of the dry and wet 6 μm nanograss glass for water and toluene. Figure S4 in Supplement 1 shows the total transmission, direct transmission, and haze for all three liquids. The direct transmission of 6 μm hazy glass at 550 nm is 0.94%, and its haze factor is 99%. When this glass is wet with water and toluene, the direct transmission increases to 44.3% and 61.5%, respectively, while the haze decreases to 55.4% and 38.3%, respectively. The total transmission also increases to near unity when it is wet (Fig. S4). As the fluid infuses the nanograss glass, the optical properties more closely resemble those of a flat fused silica, where the haze is low. The nanograss glass can switch between low and high haze states within a few seconds with the application and removal of the fluid. Visualization 1 shows a video of this transition as water is infused into glass and the water evaporates.

In conclusion, we report ultrahigh-transmission, ultrahigh-haze nanograss glass that has the ability to switch haze by applying fluid with a similar refraction index. The 4.5 μm height hazy glass showed 95.6% total transmission and 96.2% haze at 550 nm wavelength. These characteristics make the hazy glass a strong candidate to use in optoelectronic applications such as solar cells and LEDs, as well as switchable-haze smart glass that may help adjust privacy, comfort, or temperature.

Funding. National Science Foundation (NSF) (1552712).

Acknowledgment. The authors thank the Mascaro Center for Sustainable Innovation for their support.

See Supplement 1 for supporting content.

REFERENCES

1. R. B. Wehrspohn, U. Rau, and A. Gombert, *Photon Management in Solar Cells* (Wiley, 2016).
2. J. R. Nagel and M. A. Scarpulla, Opt. Express **18**, A139 (2010).
3. C. van Lare, F. Lenzmann, M. A. Verschuuren, and A. Polman, Nano Lett. **15**, 4846 (2015).
4. A. Tagaya, M. Nagai, Y. Koike, and K. Yokoyama, Appl. Opt. **40**, 6274 (2001).
5. E. Kim, H. Cho, K. Kim, T.-W. Koh, J. Chung, J. Lee, Y. Park, and S. Yoo, Adv. Mater. **27**, 1624 (2015).
6. T.-W. Koh, J. A. Spechler, K. M. Lee, C. B. Arnold, and B. P. Rand, ACS Photon. **2**, 1366 (2015).
7. Y. Yao, J. Tao, J. Zou, B. Zhang, T. Li, J. Dai, M. Zhu, S. Wang, K. K. Fu, D. Henderson, E. Hitz, J. Peng, and L. Hu, Energy Environ. Sci. **9**, 2278 (2016).
8. Z. Fang, H. Zhu, Y. Yuan, D. Ha, S. Zhu, C. Preston, Q. Chen, Y. Li, X. Han, S. Lee, G. Chen, T. Li, J. Munday, J. Huang, and L. Hu, Nano Lett. **14**, 765 (2014).
9. H.-T. Chou, Y.-C. Chen, C.-Y. Lee, H.-Y. Chang, and N.-H. Tai, Sol. Energy Mater. Sol. Cells **166**, 45 (2017).
10. P. Gould, Mater. Today **6**, 44 (2003).
11. X. Gong, J. Li, S. Chen, and W. Wen, Appl. Phys. Lett. **95**, 251907 (2009).
12. D. Cupelli, F. P. Nicoletta, S. Manfredi, G. D. Filpo, and G. Chidichimo, Sol. Energy Mater. Sol. Cells **93**, 329 (2009).
13. A. Piccolo, Energy and Buildings **42**, 1409 (2010).
14. M.-H. Yeh, L. Lin, P.-K. Yang, and Z. L. Wang, ACS Nano **9**, 4757 (2015).
15. Y. Kim, D. Jung, S. Jeong, K. Kim, W. Choi, and Y. Seo, Curr. Appl. Phys. **15**, 292 (2015).
16. S. Park and J. W. Hong, Thin Solid Films **517**, 3183 (2009).
17. X. Ye, X. Jiang, J. Huang, F. Geng, L. Sun, X. Zu, W. Wu, and W. Zheng, Sci. Rep. **5**, 13023 (2015).
18. K. Nojiri, *Dry Etching Technology for Semiconductors* (Springer, 2012).
19. G. Han, S. Zhang, P. P. Boix, L. H. Wong, L. Sun, and S.-Y. Lien, Prog. Mater. Sci. **87**, 246 (2017).
20. A. Zitzler-Kunkel, M. R. Lenze, N. M. Kronenberg, A.-M. Krause, M. Stolte, K. Meerholz, and F. Würthner, J. Chem. Mater. **26**, 4856 (2014).
21. N. Sahraei, K. Forberich, S. Venkataraj, A. G. Aberle, and M. Peters, Opt. Express **22**, A53 (2014).
22. C. K. Carniglia, Opt. Eng. **18**, 182104 (1979).
23. D. R. Lida, *CRC Handbook of Chemistry and Physics*, 88th ed. (CRC Press, 2007).
24. M. Zeman, R. A. C. M. M. van Swaaij, J. W. Metselaar, and R. E. I. Schropp, J. Appl. Phys. **88**, 6436 (2000).
25. J. Springer, A. Poruba, and M. Vanecek, J. Appl. Phys. **96**, 5329 (2004).
26. A. Poruba, A. Fejfar, Z. Remeš, J. Špringer, M. Vaněček, J. Kočka, J. Meier, P. Torres, and A. Shah, J. Appl. Phys. **88**, 148 (2000).
27. J. Drelich and E. Chibowski, Langmuir **26**, 18621 (2010).